Realization of white organic light-emitting devices using single green emitter by coupled microcavities with two modes

2015 Appl. Phys. Express 8 022103

(http://iopscience.iop.org/1882-0786/8/2/022103)

Applied Physics Express **8**, 022103 (2015)
http://dx.doi.org/**10.7567/APEX.8.022103**

Realization of white organic light-emitting devices using single green emitter by coupled microcavities with two modes

Yue Yu, Zhaoxin Wu*, Bo Jiao, Lin Ma, Han Chen, and Xun Hou

Key Laboratory of Photonics Technology for Information, School of Electronic and Information Engineering, Xi'an Jiaotong University, Xi'an 710049, P. R. China
E-mail: zhaoxinwu@mail.xjtu.edu.cn

Received November 21, 2014; accepted December 26, 2014; published online January 22, 2015

We fabricated a novel white organic light-emitting diode (WOLED) structure based on a single green emitting layer through coupled microcavities with two modes. By optical simulation and experiment, we showed that the two resonant modes can be adjusted by varying the thickness of the special layer to shape white light using only a single green emitter. Utilizing tris(8-hydroxyquinoline)aluminum (Alq_3) as an emitting layer, we obtained a series of WOLEDs whose Commission Internationale de L'Eclairage (CIE) coordinates are on the Planckian curve from (0.334, 0.343) to (0, 412, 0.393) with current efficiencies in the range of 1.45–2.52 cd A^{-1}. A maximum current efficiency of 10.12 cd A^{-1} and warm white emission at CIE (0.439, 0.461) have been demonstrated using bis(2-phenylpyridine)(acetylacetonate)iridium(III) [$Ir(ppy)_2(acac)$] as an emitter material.

Recently, there has been growing interest in white organic light-emitting diodes (WOLEDs) owing to their potential to replace commercial sources for lighting applications.[1–5] The most conventional architectures of such devices consist of two or three emitting phosphorescent or fluorescent molecules and expensive indium tin oxide (ITO), thus leading to complicated processes and high fabrication costs.[6,7] Thus, the development of a low-cost and easy fabrication technology could create new opportunities for lighting applications. From the viewpoint of optical optimization, it is effective to improve luminance and control color through microcavity resonators.[8–10] Researchers have demonstrated that microcavity resonators can be efficient in enhancing efficiency and narrowing the electroluminescent spectra of monochrome OLEDs.[11,12] On the other hand, the use of a microcavity resonator can also be considered as one of the effective ways to realize organic WOLEDs. Dodabalapur et al. utilized a dielectric mirror and an Al cathode to demonstrate that a multimode resonant microcavity is effective for controlling the color of OLEDs, including white ones.[13,14] The structure of these devices is almost the same as that of usual single-mode cavity devices; however, the thickness of the cavity is so large that it has several resonant modes, thus inevitably leading to complicated processes. Therefore, two or more resonant peaks appear in the external spectrum, and mixed colors such as white are realized. In addition, each resonant peak position in these devices cannot be adjusted arbitrarily, because all of the resonant modes are dependent on each other. By changing the thickness of an organic layer such as a hole transport layer to control the cavity length, Fan et al. realized a top-emitting microcavity WOLED with several resonant modes;[15] the electrical characteristics of the device with a thick hole transport layer are inferior to those of a conventional architecture. Mazzeo et al. reported an innovative high-performance ITO-free WOLED architecture based on the coupling of two or three organic microcavities consisting of only thermally evaporated metallic and organic layers.[16,17] The emitting layer (EML) that they used still contained two or three emitting phosphorescent or fluorescent molecules. The complicated EML itself emits white light.

In this study, we demonstrate an innovative method to realize white emission based on a single green EML through coupled microcavities, which is a low-cost and easy fabrication method. By carefully controlling the thickness of each layer, the Commission Internationale de L'Eclairage (CIE) coordinates of the WOLEDs based on tris(8-hydroxyquinoline)aluminum (Alq_3) can be accurately adjusted along the Planckian curve from (0.334, 0.343) to (0, 412, 0.393). Furthermore, these devices show stable CIE coordinates at various applied voltages. We also achieve a maximum current efficiency of 10.12 cd A^{-1} and warm white emission at CIE (0.439, 0.461) using bis(2-phenylpyridine)(acetylacetonate)iridium(III) [$Ir(ppy)_2(acac)$] as an emitter material.

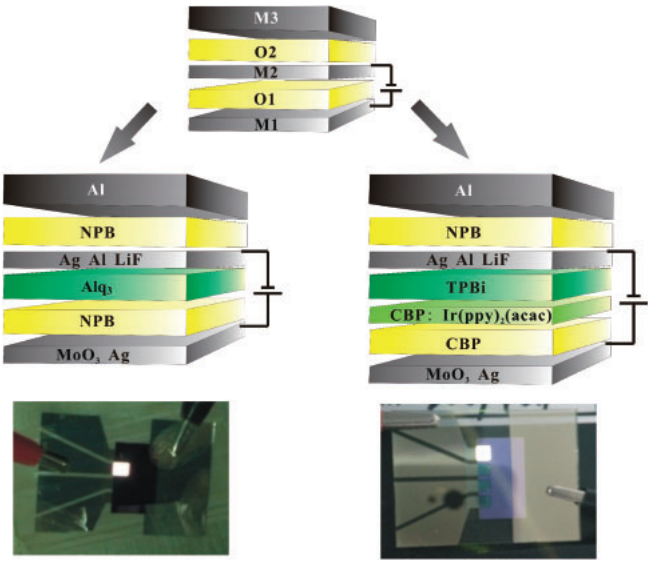

Fig. 1. Schematic view of the coupled-microcavity WOLEDs and emission photographs of devices C (left) and G (right).

As shown in Fig. 1, the structure is deposited on a transparent substrate with the following configuration: glass/M1/O1/M2/O2/M3. The device contains two coupled microcavities composed of two metallic mirrors (M1 and M2 or M2 and M3) separated by an organic layer (O1 or O2). The common metallic mirror M2 works as the coupler of the microcavities, and the degree of coupling is determined by its thickness. M1 is a semitransparent Ag anode, M2 is a semitransparent Ag cathode, and M3 is a thick reflective Al layer. O1 is an organic stack including an EML, and O2 is an optical adjustment layer, for instance, 4,4′-bis[*N*-(1-naphthyl)-*N*-phenyl-amino]biphenyl (NPB). In this work, we used the

common material Alq_3 or $Ir(ppy)_2(acac)$ as a green-emitting material. The configuration of O1 is molybdenum trioxide (MoO_3)/NPB/Alq_3/LiF/Al or MoO_3/NPB/4,4′-bis(*N*-carbazolyl)biphenyl (CBP): $Ir(ppy)_2(acac)$/1,3,5-tris(1-phenyl-1*H*-benzimidazol-2-yl)benzene (TPBi)/LiF/Al, where MoO_3 was used as the hole injection layer (HIL), NPB was used as the hole transport layer (HTL), Alq_3 and TPBi were used as electron transport layers (ETLs), and thin LiF and Al were used as electron injection layers (EILs).

OLEDs were fabricated onto a cleaned glass substrate by thermal evaporation at a pressure of 1×10^{-3} Pa without vacuum break. The thickness of the films was determined using a quartz-crystal sensor. The active area of the devices was $3 \times 4\,mm^2$ for all the samples studied in this work. The voltage–current density (*V*–*J*) and voltage–brightness (*V*–*L*) characteristics of the devices were measured with a Keithley 2602 source meter. All the measurements were carried out at room temperature under ambient conditions. The PR650 spectrophotometer and fiber optic spectrometer were utilized to measure the electroluminescent (EL) spectra.

In order to optimize the geometrical configuration and obtain simultaneously a white-emitting spectrum, an optical simulation program is compiled to simulate the relationship between the spectra of these devices and the thicknesses of layers within these devices by transmission-matrix electromagnetic calculations.[16,18] We assumed constant and non-dispersive refractive indices of $n = 1$, 1.56, and 1.8 for air, glass, and ITO layers, respectively. For other layers, we determined the complex refractive index of $\hat{n} = n + ik$ by spectroscopic ellipsometry. (For example, $\lambda = 540$ nm, organic material: $1.71 + 0.0282i$, Al: $0.912 + 6.55i$, Ag: $0.102 + 3.91i$.) The refractive index data were considered as the material parameters for the simulation.

To investigate the relationship between the spectra and the thicknesses of the Ag cathode, HTL NPB, and optical adjustment layer NPB, we designed three groups of devices. The thicknesses of the EML and Ag anode are fixed to ensure constant electrical characteristics and index of transmittance. Figure 2(a) shows the experimental and simulation spectra of a series of devices: glass/Ag (20 nm)/MoO_3 (3 nm)/NPB (45 nm)/Alq_3 (55 nm)/LiF (1 nm)/Al (3 nm)/Ag (15, 20, 25, 30, 50 nm)/NPB (95 nm)/Al (100 nm). The thickness of the semitransparent Ag cathode has a considerable influence on resonant peaks of the device. The thickness of the Ag cathode determines the distance between two resonant peaks. As the thickness of the Ag cathode increases from 15 to 30 nm, the wavelength of the resonant peak in the short-wave area increases from 484 to 500 nm, while that in the long-wave area decreases from 628 to 568 nm. Additionally, in the device with a 50 nm Ag cathode, we obtain only one resonant peak in its spectra. This is because the cathode is so thick that it is opaque, resulting in the dysfunction of the optical adjustment layer. Furthermore, the simulation results agree very well with the experimental EL spectrum, as shown in Fig. 2(a). According to the simulation and experimental results, by varying the thickness of the Ag cathode, the position of the two wavelengths can be tuned over the entire visible range. As for WOLEDs, the device can be designed to amplify only the modes in the blue and red regions when the thickness of the Ag cathode is about 20 to 25 nm. We designed another series of

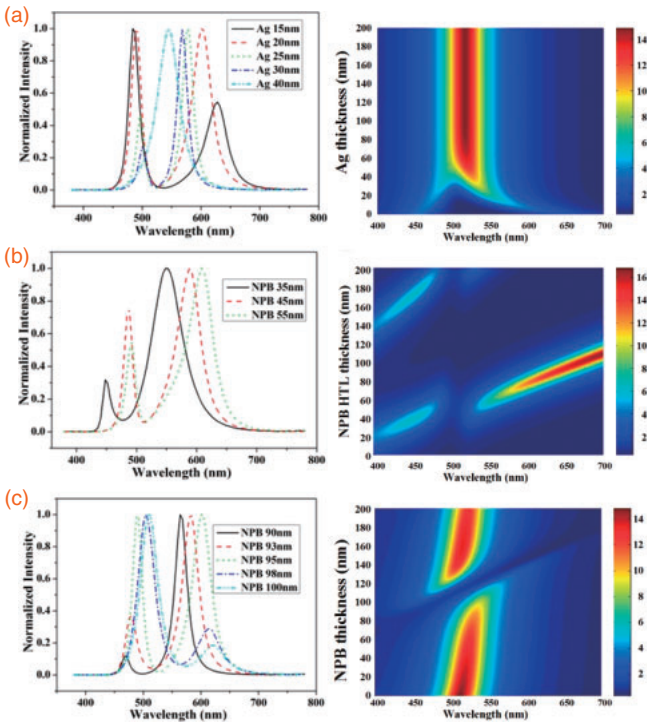

Fig. 2. Experimental and simulation spectra of coupled-microcavity devices.

devices as below to investigate the relationship between the spectra and the thickness of the HTL NPB: glass/Ag (20 nm)/MoO_3 (3 nm)/NPB (35, 45, 55 nm)/Alq_3 (55 nm)/LiF (1 nm)/Al (3 nm)/Ag (20 nm)/NPB (90 nm)/Al (100 nm). Experimental and simulation results are shown in Fig. 2(b). We obtain three pairs of resonant peaks in the spectra according to three different HTL thicknesses. At HTL thicknesses of 35, 45, and 55 nm, the relative resonant peak pairs are 448 and 552 nm, 488 and 588 nm, and 492 and 608 nm, respectively. With the decrease in HTL thickness, the wavelengths of the resonant peaks in the spectra decrease. The simulation results also indicate that the HTL thickness determines the integral locations of two resonant peaks in the spectra, as shown in Fig. 2(b). In order to obtain WOLEDs, an HTL NPB thickness of around 45 nm is used; thus, two resonant peaks appear in the blue and red regions. Figure 2(c) shows the impact of the thickness of the optical adjustment layer NPB on the spectra; both experimental and simulation results are given. The structures of this group of devices are glass/Ag (20 nm)/MoO_3 (3 nm)/NPB (40 nm)/Alq_3 (55 nm)/LiF (1 nm)/Al (3 nm)/Ag (20 nm)/NPB (90, 95, 98, 100, 110 nm)/Al (100 nm). When the thickness of the optical adjustment layer increases, the intensity of the resonant peak in the long-wave area increases, whereas that in the short-wave area decreases. Moreover, the integral locations of two resonant peaks in the spectra move toward the long-wave direction as the thickness of the optical adjustment layer increases. The simulation results also show the variation tendency as we discussed above. We can obtain a balanced WOLED by carefully selecting the thickness of the optical adjustment layer NPB.

By optical simulation and experiment, we show that the two resonant modes can be adjusted by varying the thickness of the special layer. As for white OLEDs, at least two

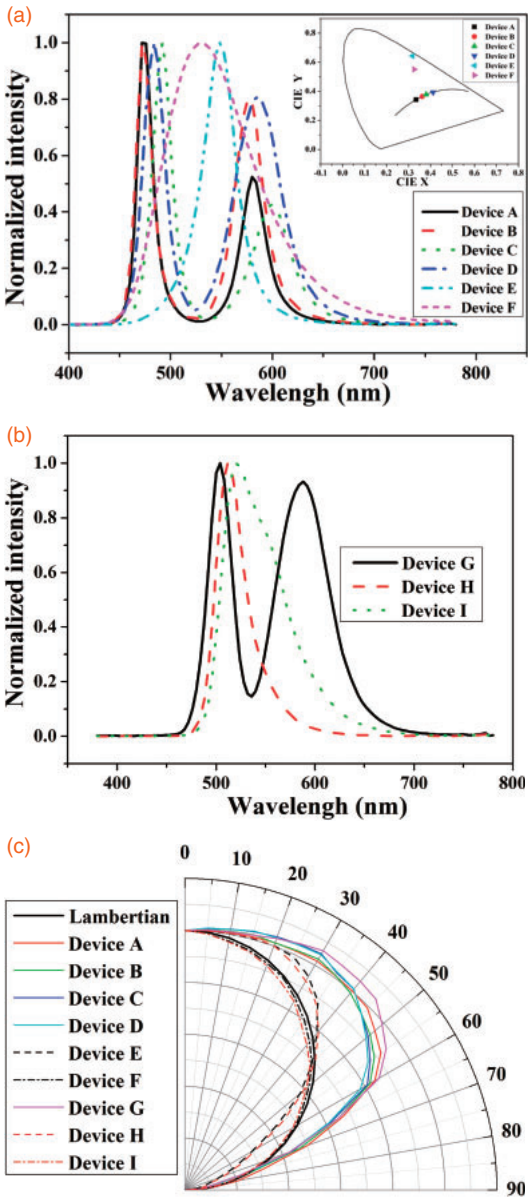

Fig. 3. (a) EL spectra and CIEs of devices A–F at 8 V. (b) EL spectra of devices G–I at 8 V. (c) Measured angular distribution of devices A–I.

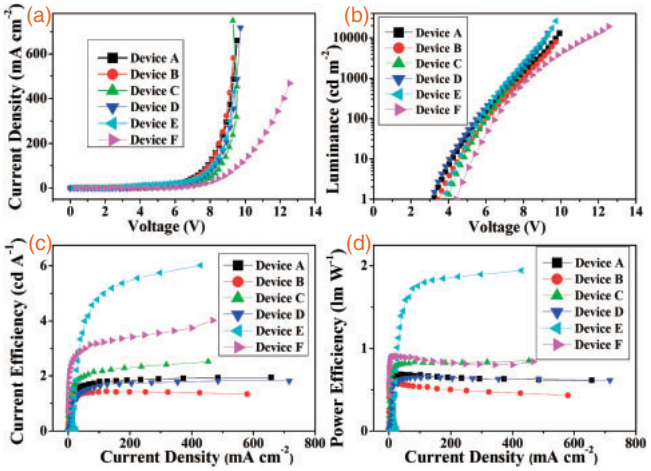

Fig. 4. (a) Current density–voltage curves. (b) Brightness–voltage curves. (c) Current efficiency–current density curves. (d) Power efficiency–current density curves for devices A–F.

resonant peaks in the emission spectra are required. According to the simulation and experimental results, two resonant peaks appear in the blue and red regions when the thickness of the Ag cathode is between 20 and 25 nm, the thickness of the HTL NPB is around 45 nm, and the thickness of the optical adjustment layer NPB is between 90 and 110 nm. On the basis of the laws of spectral change, we fabricated several devices, whose thicknesses were precisely controlled. The configuration details of these devices are shown as below:

device A: glass/Ag (20 nm)/MoO_3 (3 nm)/NPB (44 nm)/ Alq_3 (55 nm)/LiF (0.5 nm)/Al (3 nm)/Ag (20 nm)/ NPB (98 nm)/Al (150 nm);

device B: glass/Ag (20 nm)/MoO_3 (3 nm)/NPB (44 nm)/ Alq_3 (55 nm)/LiF (0.5 nm)/Al (3 nm)/Ag (21 nm)/ NPB (96 nm)/Al (150 nm);

device C: glass/Ag (20 nm)/MoO_3 (3 nm)/NPB (46 nm)/ Alq_3 (55 nm)/LiF (0.5 nm)/Al (3 nm)/Ag (21 nm)/ NPB (96 nm)/Al (150 nm);

device D: glass/Ag (20 nm)/MoO_3 (3 nm)/NPB (45 nm)/ Alq_3 (55 nm)/LiF (0.5 nm)/Al (3 nm)/Ag (22 nm)/ NPB (100 nm)/Al (150 nm);

device E: glass/Ag (20 nm)/MoO_3 (3 nm)/NPB (44 nm)/ Alq_3 (55 nm)/LiF (0.5 nm)/Al (150 nm);

device F: glass/ITO/MoO_3 (3 nm)/NPB (44 nm)/ Alq_3 (55 nm)/LiF (0.5 nm)/Al (150 nm).

Among these devices, devices A, B, C, and D are based on coupled microcavities. For comparison, we also prepared device E with only a single microcavity and reference cavityless device F. The spectra and CIE coordinates of these devices are shown in Fig. 3(a). From the results, we could see that devices A, B, C, and D based on coupled microcavities realized white emission. The CIE coordinates of the white lights produced by our devices for illumination applications can be accurately adjusted along the Planckian curve from (0.334, 0.343) to (0, 412, 0.393). Furthermore, these devices show stable CIE coordinates at various applied voltages. For example, the CIE coordinates of device A change from (0.334, 0.343) at 4 V to (0.339, 0.345) at 9 V, in which the change of the CIE coordinates is only (0.005, 0.002). We therefore conclude that this structure of coupled microcavities helps stabilize the color coordinates of WOLEDs. To obtain power efficiency and external quantum efficiency (EQE), as shown in Fig. 3(c), the wavelength- and angle-dependent integrals have to be taken into account.[12,19,20] Figure 4 shows the current density–voltage–luminance–efficiency (J–V–L–η) characteristics of these devices. The key device performance parameters and EL emission characteristics are summarized in Table I. The current and power efficiencies of devices A–D are in the ranges of 1.45–2.52 cd A^{-1} and 0.62–0.86 lm W^{-1}, respectively. Notably, device C achieves the best EL performance, with a maximum EQE as high as 1.24%, a maximum current efficiency of 2.52 cd A^{-1}, a maximum power efficiency of 0.86 lm W^{-1}, and white emission at CIE (0.380, 0.378). The EQEs of these coupled-microcavity devices can be compared with that of device F and are slightly lower than that of device E.

In order to improve the performance parameter, we employ an efficient green phosphorescent emitter material, $Ir(ppy)_2(acac)$, and the host CBP. By carefully controlling

Table I. EL performance.

Device	λ_{max}^{EL} a) (nm)	V_{on} b) (V)	L_{max} c) (cd m^{-2})	η_{ext} d) (%)	η_c d) (cd A^{-1})	η_p d) (lm W^{-1})	CIE a) (x, y)	Current density a) (mA cm^{-2})
A	474/580	3.3	12803	0.92	1.95	0.62	(0.334, 0.343)	102.2
B	472/576	3.4	7781	0.57	1.45	0.54	(0.362, 0.364)	98.4
C	492/600	3.9	11425	1.24	2.52	0.86	(0.380, 0.378)	52.5
D	484/586	3.5	13046	0.73	1.82	0.62	(0.412, 0.393)	75.7
E	549	3.6	25786	1.43	6.02	1.94	(0.318, 0.643)	93.9
F	529	4.2	18822	1.27	4.02	0.84	(0.326, 0.551)	23.6
G	502/589	2.8	34129	3.52	10.12	4.98	(0.439, 0.461)	223.5
H	512	2.6	75950	10.61	34.82	25.69	(0.175, 0.685)	251.2
I	520	3.2	97124	15.38	57.42	38.67	(0.282, 0.648)	19.7

a) Values collected at 8 V. b) Turn-on voltage at 1 cd m^{-2}. c) Maximum luminance. d) Values collected at a peak efficiency.

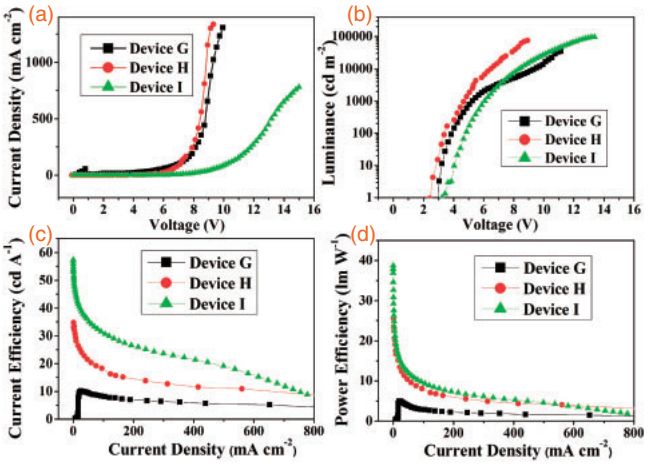

Fig. 5. (a) Current density–voltage curves. (b) Brightness–voltage curves. (c) Current efficiency–current density curves. (d) Power efficiency–current density curves for devices G–I.

the thickness of each layer, we ultimately obtain WOLEDs in the yellowish-white color region. The configuration details of such devices are shown as below:

device G: glass/Ag (22 nm)/MoO_3 (10 nm)/NPB (35 nm)/ CBP: Ir(ppy)$_2$(acac) (8 wt %) (15 nm)/TPBi (45 nm)/ LiF (0.5 nm)/Al (3 nm)/Ag (16 nm)/NPB (96 nm)/ Al (150 nm);

device H: glass/Ag (22 nm)/MoO_3 (10 nm)/NPB (35 nm)/ CBP: Ir(ppy)$_2$(acac) (8 wt %) (15 nm)/TPBi (45 nm)/ LiF (0.5 nm)/Al (150 nm);

device I: glass/ITO/MoO_3 (10 nm)/NPB (35 nm)/CBP: Ir(ppy)$_2$(acac) (8 wt %) (15 nm)/TPBi (65 nm)/ LiF (0.5 nm)/Al (150 nm).

Device G is a coupled-microcavity device. For comparison, we also prepared device H with only a single microcavity and reference cavityless device I. The spectra of these devices are shown in Fig. 3(b). Figure 5 shows the J–V–L–η characteristics of these devices. The key device performance parameters and EL emission characteristics are also summarized in Table I. Device G achieves a maximum EQE as high as 3.52%, a maximum current efficiency of 10.12 cd A^{-1}, a maximum power efficiency of 4.98 lm W^{-1}, and warm white emission at CIE (0.439, 0.461). However, owing to the narrow original spectra of Ir(ppy)$_2$(acac) and the weak emission in the blue region, the efficiency of coupled-microcavity device G is much lower than those of device H with a single microcavity and reference cavityless device I.

In summary, we have developed an effective approach to fabricate white OLEDs based on a simple green emitting layer through coupled microcavities. We also proposed an optical model for simulation and investigated the relationship between resonant peaks and the thickness of the special layer in the device. By carefully controlling the thickness of each layer, a maximum current efficiency of 2.52 cd A^{-1} with white emission at CIE (0.380, 0.378) based on Alq_3 and a maximum current efficiency of 10.12 cd A^{-1} with warm white emission at CIE (0.439, 0.461) were obtained using Ir(ppy)$_2$(acac) as an emitter material.

Acknowledgments This work was financially supported by the Basic Research Program of China (2013CB328705), the National Natural Science Foundation of China (Grant Nos. 61275034 and 61106123), the Ph.D. Programs Foundation of the Ministry of Education of China (Grant No. 20130201110065), and Fundamental Research Funds for the Central Universities (Grant No. xjj2012087).

1) J. Kido, M. Kimura, and K. Nagai, Science **267**, 1332 (1995).
2) Y. Sun and S. R. Forrest, Nat. Photonics **2**, 483 (2008).
3) E. L. Williams, K. Haavisto, J. Li, and G. E. Jabbour, Adv. Mater. **19**, 197 (2007).
4) S. Reineke, F. Lindner, G. Schwartz, N. Seidler, K. Walzer, B. Lussem, and K. Leo, Nature **459**, 234 (2009).
5) M. G. Helander, Z. B. Wang, J. Qiu, M. T. Greiner, D. P. Puzzo, Z. W. Liu, and Z. H. Lu, Science **332**, 944 (2011).
6) K. Fehse, K. Walzer, K. Leo, W. Lövenich, and A. Elschner, Adv. Mater. **19**, 441 (2007).
7) C. Piliego, M. Mazzeo, M. Salerno, R. Cingolani, G. Gigli, and A. Moro, Appl. Phys. Lett. **89**, 103514 (2006).
8) E. M. Pucell, Phys. Rev. **69**, 681 (1946).
9) S. Stelitano, G. D. Luca, and S. Savasta, Appl. Phys. Lett. **95**, 093303 (2009).
10) C. L. Lin, H. W. Lin, and C. C. Wu, Appl. Phys. Lett. **87**, 021101 (2005).
11) E. Lee, Vacuum **83**, 848 (2009).
12) R. Meerheim, R. Nitsche, and K. Leo, Appl. Phys. Lett. **93**, 043310 (2008).
13) A. Dodabalapur, L. J. Rothberg, and T. Miller, Appl. Phys. Lett. **65**, 2308 (1994).
14) A. Dodabalapur, L. J. Rothberg, R. H. Jordan, T. M. Miller, R. E. Slusher, and J. M. Phillips, J. Appl. Phys. **80**, 6954 (1996).
15) Y. Fan, H. Zhang, J. Chen, and D. Ma, Org. Electron. **14**, 1898 (2013).
16) M. Mazzeo, F. D. Sala, F. Mariano, G. Melcarne, S. D' Agostino, Y. Duan, R. Cingolani, and G. Gigli, Adv. Mater. **22**, 4696 (2010).
17) M. Mazzeo, F. Mariano, A. Genco, S. Carallo, and G. Gigli, Org. Electron. **14**, 2840 (2013).
18) S. Hofmann, M. Thomschke, P. Freitag, M. Furno, B. Lüssem, and K. Leo, Appl. Phys. Lett. **97**, 253308 (2010).
19) N. C. Greenham, R. H. Friend, and D. D. C. Bradley, Adv. Mater. **6**, 491 (1994).
20) I. Tanaka and S. Tokito, Jpn. J. Appl. Phys. **43**, 7733 (2004).